Supplementary material:
Irreversible hydrodynamic trapping by surface rollers

Alexander Chamolly,[1,*] Eric Lauga,[1,†] and Soichiro Tottori[2,‡]

[1]*Department of Applied Mathematics and Theoretical Physics, University of Cambridge, Cambridge CB3 0WA, United Kingdom*
[2]*Cavendish Laboratory, Department of Physics, University of Cambridge, CB3 0HE, United Kingdom*

(Dated: February 13, 2020)

I. VERIFICATION OF THE FINITE-ELEMENT METHOD

In order to verify the numerical accuracy of our finite-element routine, we simulated the force on the translating and rotating ellipsoids, calculated the rotation-translation coupling rate, and compared these results with the data by Goldman *et al.* [2] in Fig. S1. The mesh was refined until the deviation from the Goldman's data fell below 1% at the gap width $\delta/a = 0.005004$.

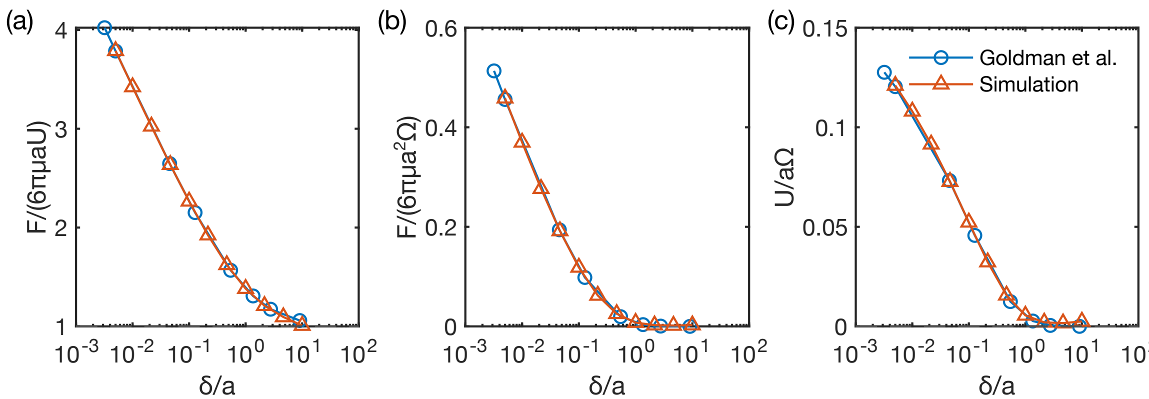

FIG. S1: Comparison of our numerical method with the results by Goldman et al. for $a/b = 1$ [2]. (a) Normalised force on a translating sphere, (b) normalised force on a rotating sphere, and (c) force-free rotation-translation coupling rate as a function of the dimensionless gap width δ/a.

II. ANALYSIS OF THE FLOW DISTURBANCE DUE TO FINITE CARGO SIZE

In this article, we employ a simplified, minimal approach to calculate the trajectory of the cargo particle in the flow created by the roller. Specifically, we calculate the flow field in the absence of any cargo particle using a finite-element routine, and then assume that the cargo simply follows the streamlines of this flow (except when altered by steric interactions). We employ this methodology since dynamic simulations in this geometry require computation times on the order of weeks to months for each individual data point, which is prohibitively expensive. However, it is of course still necessary to quantify the error incurred by this simplification.

In order to assert the accuracy of our analysis, we calculate the flow field in the presence of a force- and torque-free cargo particle at six judiciously chosen positions and parameter configurations using the same finite-element routine with the remaining boundary conditions unchanged. These parameter configurations are listed on the left side of Table S1. Here, (a) to (d) are chosen to match the data points analysed in detail in Fig. 5 of the main text, while (e) and (f) represent an extreme point in the top right of the phase diagram Fig. 4 of the main text, where we expect our analysis to be least accurate. We assume in each case that the cargo follows streamlines according to our minimal

* ajc297@cam.ac.uk
† e.lauga@damtp.cam.ac.uk
‡ st607@cam.ac.uk

	b/a	r/a	l/a (see text)	Trapped?	Cargo location	Δ^2	β
(a)	0.5	0.05	0.07	No	Centre of squeezing	0.1300	0.14°
(b)	0.5	0.10	0.07	Yes	Centre of squeezing	0.1203	0.03°
(c)	0.5	0.10	0.07	Yes	Halfway up vortex	0.0033	0.16°
(d)	0.5	0.25	0.07	No	Centre of squeezing	0.0179	0.10°
(e)	0.125	0.25	0.15	Yes	Centre of squeezing	0.0818	0.04°
(f)	0.125	0.25	0.15	Yes	Halfway up vortex	0.0033	0.67°

TABLE S1: Parameter configurations for the verification of our methodology (left of double line) and two measures for the accuracy of the computed cargo velocity (right of double line).

model up to the location where we calculate the flow field exactly. The value of l/a is therefore to be understood as an identifier of the minimal model configuration that informs a particular cargo location, rather than a direct input to the numerical procedure.

As illustrated in Fig. S2, the nature of the streamline through the cargo centre is the same as in the simplified case presented in the main text in all cases considered. Furthermore, the qualitative disturbance of the flow topology due to the presence of the cargo is very small, even for a comparatively large particle with $r/a = 0.25$ as shown in Fig. S2 (d) to (f). In the cases where the cargo is located at the centre of squeezing there is no visible deformation, while in the cases where the cargo is transported upward in the vortex there is a slight bending of the streamlines immediately in contact with the particle. This is due to a rigid-body rotation that the cargo experiences due to a non-zero vorticity of the flow. Crucially, the topology of the vortex remains intact. Even in the extreme case (f) the cargo particle is located well inside the vortex, with streamlines that escape to infinity separated from the cargo surface by more one cargo radius. However, as is illustrated in case (d), the picture is less clear at the centre of squeezing, where a slight upward dislocation of the cargo might lead to trapping. This threshold may conceivably be crossed even just due to thermal noise. The boundaries of our phase diagram may therefore be slightly blurred in a real system. Nevertheless, these results provide strong evidence that our methodology classifies particle trajectories accurately.

To provide further quantitative evidence for the accuracy of the methodology, we compute the velocity of the cargo particle $\boldsymbol{u}_c$ in the cases (a) to (f) and compare it with the flow velocity $\boldsymbol{u}(\boldsymbol{x}_c)$ at the position of the cargo centre $\boldsymbol{x}_c$ calculated in the absence of the particle. Since the velocities are vectors, we compare both the normalised squared difference in magnitude $\Delta^2 = |\boldsymbol{u}_c - \boldsymbol{u}(\boldsymbol{x}_c)|^2/|\boldsymbol{u}_c|^2$, and the angle $\beta = \cos^{-1}\left(\boldsymbol{u}_c \cdot \boldsymbol{u}(\boldsymbol{x}_c)/|\boldsymbol{u}_c||\boldsymbol{u}(\boldsymbol{x}_c)|\right)$ between the velocity vectors. These results are summarised on the right side of Table S1. In all cases, the difference in direction is vanishingly small and amounts to less than 1°. The difference in magnitude is larger, especially when the cargo is located at the centre of squeezing. This is due to friction forces that could be calculated using lubrication theory. These are most significant in the cases (a) and (b) when the cargo is squeezed below the vortex while still passing close to the side of the roller, and smaller when the particle is deflected further to the side in the cases (d) and (e) and especially when it is located further away from rigid boundaries as in cases (c) and (f). Overall however the error remains small, and supports the modelling approach in the main text.

III. DERIVATION OF THE STREAMFUNCTION FOR A ROTATING RIGID DISC

The first important feature of the phase diagram is the prominence of trapping for rollers with a narrow aspect ratio. In order to elucidate this further, we begin by considering the extreme case of a rolling disc, i.e. we consider the limit $b = 0$, and in order to make analytical progress, we ignore the presence of the wall. We consider a frame in which the disc is stationary but rotating with angular velocity $\boldsymbol{\Omega} = \Omega\hat{\boldsymbol{y}}$, and scale lengths by the disc radius, a. Since the no-slip condition is applied on the disc's surface, very near to it (that is for $|y|$ small) the fluid is approximately in solid body rotation. In terms of cylindrical polar coordinates (ρ, θ, y) with $\rho^2 = x^2 + z^2$ and $\tan\theta = x/z$ we therefore seek a solution to the Stokes equations with boundary condition

$$\boldsymbol{u} = \Omega\rho\boldsymbol{e}_\theta, \quad y = 0, \rho < 1, \tag{1}$$

and flow decaying to zero at infinity. For convenience, we introduce oblate spheroidal coordinates (λ, ξ, θ) defined by

$$y = \lambda\xi, \tag{2}$$

$$\rho^2 = (\lambda^2 + 1)(1 - \xi^2), \tag{3}$$

$$\theta = \theta. \tag{4}$$

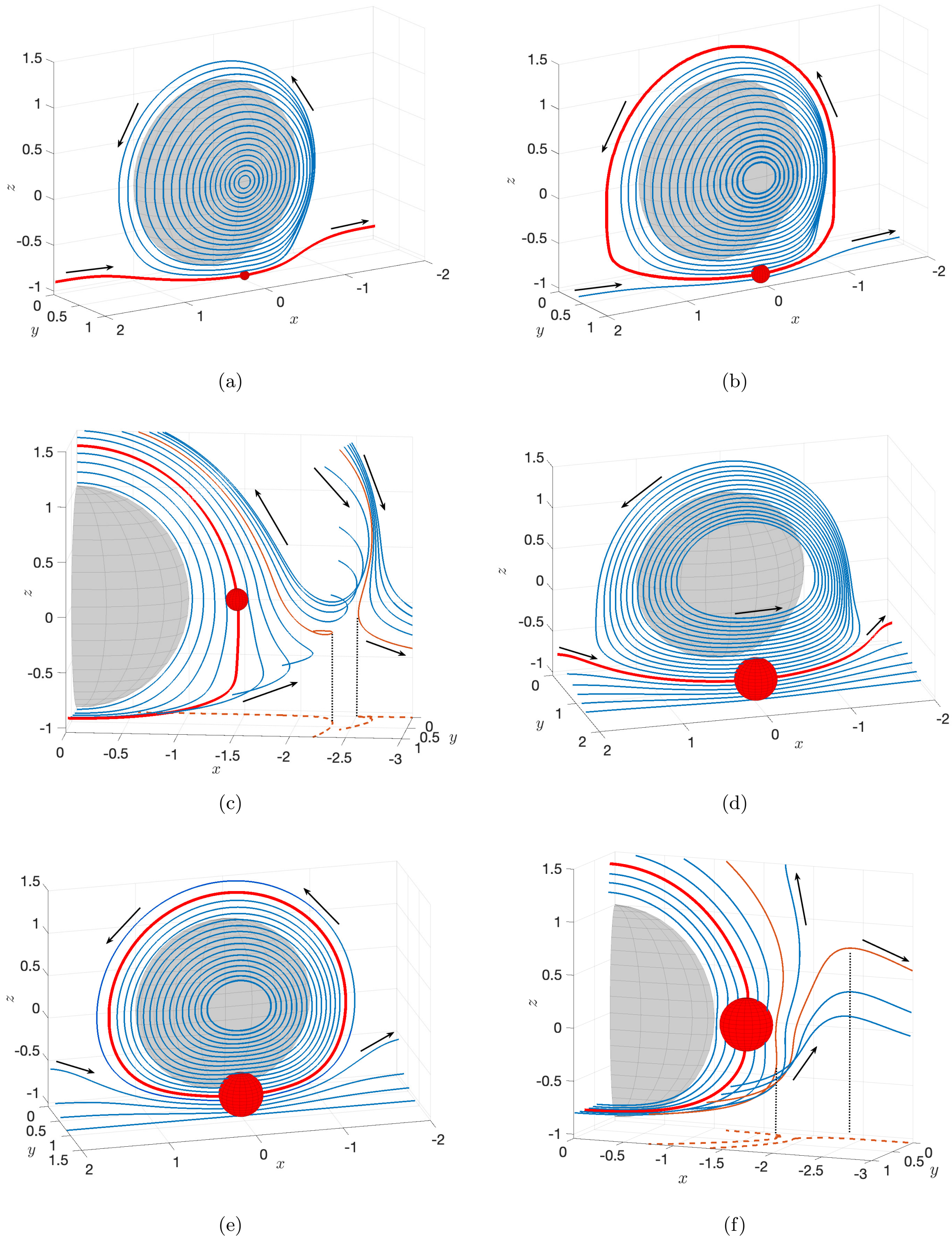

(a) (b) (c) (d) (e) (f)

FIG. S2: Numerical illustration of streamlines for each of the parameter configurations listed in Table S1. The streamline through the cargo centre is highlighted in bold red, black arrows give an indication of flow direction. In (c) and (f) the shadows of certain (orange) streamlines are drawn in dashed orange to help visualise the flow topology.

Note that λ and θ are dimensionless, while ξ has units of length. Surfaces of constant λ are oblate spheroids that are defined by the relation

$$\frac{\rho^2}{1+\lambda^2}+\frac{y^2}{\lambda^2}=1. \tag{5}$$

In particular, the degenerate case $\lambda=0$ corresponds to a disc of radius 1. Casting the problem in these coordinates therefore lends itself to a particularly convenient form of the boundary condition Eq. (1), namely

$$\boldsymbol{u}=\Omega\rho\boldsymbol{e}_\theta, \quad \lambda=0. \tag{6}$$

where $\rho(\lambda,\xi)$ is defined implicitly. It can be shown [5] that the solution is a purely azimuthal flow given

$$\boldsymbol{u}=u_\theta(\rho,\lambda)\boldsymbol{e}_\theta, \quad u_\theta=\Omega\rho\times\frac{2}{\pi}\left(\cot^{-1}\lambda-\frac{\lambda}{1+\lambda^2}\right), \tag{7}$$

which we can evaulate by using the relation

$$\lambda=\left\{\frac{1}{2}\left(\rho^2+y^2-1\right)+\frac{1}{2}\left[\left(\rho^2+y^2-1\right)^2+4y^2\right]^{1/2}\right\}^{1/2}. \tag{8}$$

Since the flow is purely azimuthal in the x-z plane, and therefore two-dimensional (2D) incompressible, we can define a streamfunction of the form $\boldsymbol{\psi}=\psi(\rho;y)\hat{\boldsymbol{y}}$ that recovers this flow field if we treat y as a parameter that labels different 'slices' of the fluid. Since $u_\theta=-\partial\psi/\partial\rho$ we have

$$\psi=\frac{2\Omega}{\pi}\int\left(\frac{\lambda}{1+\lambda^2}-\cot^{-1}\lambda\right)\rho\,\mathrm{d}\rho, \tag{9}$$

We note that Eq. (5) implies $\rho d\rho/d\lambda=\lambda+y^2/\lambda^3$ and so we can integrate Eq. (9) exactly to find

$$\psi=\frac{\Omega}{\pi}\left[-3\frac{y^2}{\lambda}+\lambda+\left(\frac{y^2}{\lambda^2}+1+3y^2-\lambda^2\right)\cot^{-1}\lambda\right], \tag{10}$$

where we choose the constant of integration such that $\psi\to 0$ as $\lambda\to\infty$. This is the streamfunction for a rotating rigid disc in a quiescent infinite fluid.

IV. DETAILS OF THE 2D SINGULARITY MODEL

A. Derivation

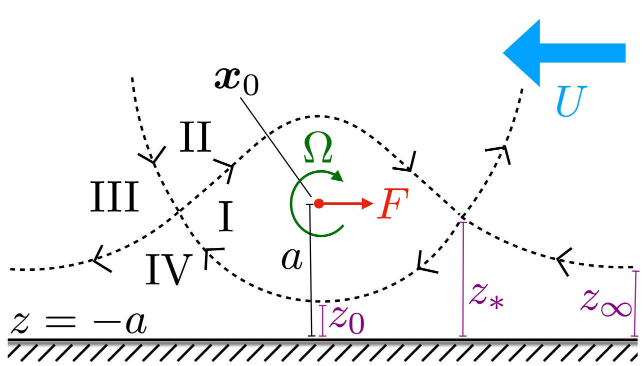

FIG. S3: Sketch of the model geometry with the separatrix streamline and stagnation points.

Here we give some additional details for the 2D singularity model. We reproduce the sketch of the 2D singularity model in Fig. S3.

The Oseen tensor for 2D Stokes flow in the x-z plane is given by[4]

$$\boldsymbol{j}(\boldsymbol{x};\boldsymbol{x}_0) = -\log r\boldsymbol{I} + \frac{\boldsymbol{r}\boldsymbol{r}}{r^2}, \tag{11}$$

where $\boldsymbol{r} = \boldsymbol{x} - \boldsymbol{x}_0$ and $r = |\boldsymbol{r}|$. Some relevant derivatives are given by

$$\partial_k j_{ij} = \frac{-r_k\delta_{ij} + r_j\delta_{ik} + r_i\delta_{jk}}{r^2} - 2\frac{r_i r_j r_k}{r^4}, \qquad \text{(force dipole)} \tag{12}$$

$$\nabla^2 j_{ij} = 2\frac{\delta_{ij}}{r^2} - 4\frac{r_i r_j}{r^4}. \qquad \text{(source dipole)} \tag{13}$$

We consider the flow due to point singularities located at $\boldsymbol{x}_0 = (0,0)$ in the presence of a rigid wall at $z = -a$ with normal $\boldsymbol{n} = (0,1)$. The flow due to a point force per unit length $\boldsymbol{F}$ is given in this geometry by

$$\boldsymbol{u}^f = \frac{\boldsymbol{F}}{8\pi\mu}\cdot\left(\boldsymbol{j} - \boldsymbol{j}^* - 2a\boldsymbol{D}\cdot\nabla(\boldsymbol{j}^*\cdot\boldsymbol{n}) + a^2\boldsymbol{D}\cdot\nabla^2\boldsymbol{j}^*\right), \tag{14}$$

where $\boldsymbol{D} = \boldsymbol{I} - 2\boldsymbol{n}\boldsymbol{n}$ and $\boldsymbol{j}^* = \boldsymbol{j}(\boldsymbol{x};\boldsymbol{D}\cdot\boldsymbol{x}_0)$. This has exactly the same structure as a point force in 3D flow [1], and by linearity the same holds true for any higher order singularities. For a force parallel to the wall in the positive x-direction the expression in Eq. (14) evaluates to

$$\boldsymbol{u}^f = \frac{F}{8\pi\mu}\begin{pmatrix} -\log r + \log R + \frac{x^2}{r^2} - \frac{x^2}{R^2} - \frac{2a(z+a)}{R^2} + \frac{4ax^2(z+a)}{R^4} \\ \frac{xz}{r^2} - \frac{xz}{R^2} + \frac{4ax(z+a)(z+2a)}{R^4} \end{pmatrix}, \tag{15}$$

where $r^2 = x^2 + z^2$, and $R^2 = x^2 + (z+2a)^2$. 2D Stokes flow is incompressible and thus admits a streamfunction ψ such that $\boldsymbol{u} = (\psi_z, -\psi_x)$. For the force parallel to the wall we then have

$$\psi^f = \frac{F}{8\pi\mu}\left(z\log\frac{R}{r} + \frac{2a(z+a)(z+2a)}{R^2}\right). \tag{16}$$

For the flow due to a point vortex in the $x-z$ plane we consider the addition of a hypothetical y-axis with $\boldsymbol{\Omega} = (0, a\Omega, 0)$ oriented along that axis. With this setup $\Omega > 0$ corresponds to a clockwise rotation in the $x-z$ plane and thus rolling in the positive x-direction. The flow is given by

$$\boldsymbol{u}^r = -\frac{1}{2}(\boldsymbol{\Omega}\times\nabla)\cdot\boldsymbol{j} + \frac{1}{2}(\boldsymbol{\Omega}\times\nabla)\cdot\boldsymbol{j}^* - (\boldsymbol{n}\times\boldsymbol{\Omega}\,\boldsymbol{n} + \boldsymbol{n}\,\boldsymbol{n}\times\boldsymbol{\Omega}) : \nabla\boldsymbol{j}^* + h(\boldsymbol{n}\times\boldsymbol{\Omega})\cdot\nabla^2\boldsymbol{j}^*. \tag{17}$$

This evaluates to the following flow in the x-z plane:

$$\boldsymbol{u}^r = \Omega a\begin{pmatrix} \frac{z}{r^2} - \frac{z}{R^2} + \frac{4x^2(z+a)}{R^4} \\ -\frac{x}{r^2} + \frac{x}{R^2} + \frac{4x(z+a)(z+2a)}{R^4} \end{pmatrix}. \tag{18}$$

The corresponding streamfunction is

$$\psi^r = \Omega a\left(-\log\frac{R}{r} + \frac{2(z+a)(z+2a)}{R^2}\right), \tag{19}$$

which is actually quite similar to ψ^f since similar image singularities are required for this solution. Finally we note that the streamfunction for a constant background flow in the negative x-direction $\boldsymbol{u}^b = (-U, 0)$ is

$$\psi^b = -U(z+a). \tag{20}$$

Most of these results have been derived previously, e.g. in [3]. All streamfunctions are defined so that they satisfy $\psi = 0$ on the wall.

We scale lengths by $a = 1$ from this point onwards and furthermore introduce the parameters $\eta = F/8\pi\mu a\Omega$ and $\gamma = U/a\Omega$ denoting the relative strength of the various terms. The combined and rescaled streamfunction is then

$$\psi = (\eta z - 1)\log\frac{R}{r} + \frac{2(1+\eta)(z+1)(z+2)}{R^2} - \gamma(z+1), \tag{21}$$

as claimed in the main text. In the following, we analyse the stagnation points and topology of the streamlines in the two cases $\eta = 0$ (force-free) and $\eta > 0$ (with force).

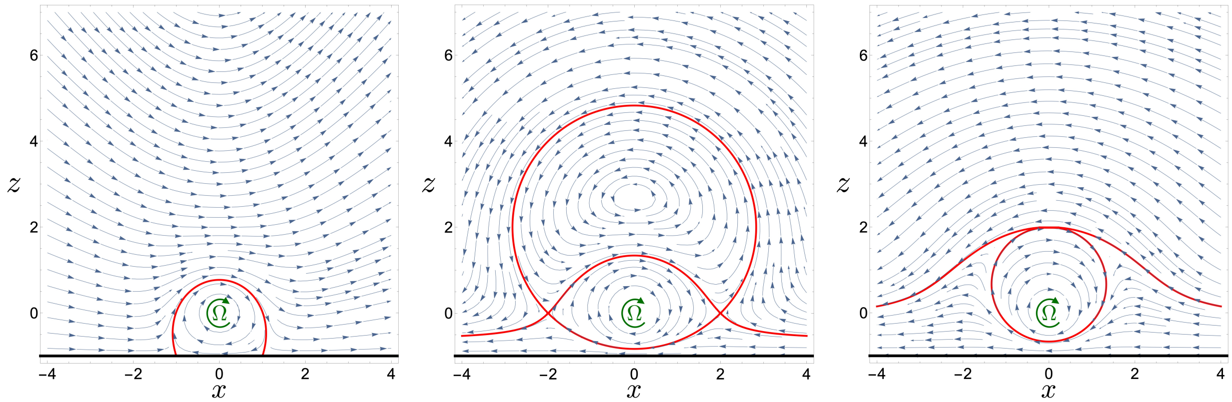

(a) $\gamma = 0$ (b) $\gamma = 0.25$ (c) $\gamma = 3/8$

FIG. S4: Streamlines for $\eta = 0$ ((no force). The separatrix streamline is indicated in bold red. For $\gamma > 0$ we see that it is squeezed below the singularity.

B. No force, $\eta = 0$

Let us first consider the case of a force-free roller, i.e. $\eta = 0$. Some sample streamlines are plotted in Figure S4. Our first goal is to find the stagnation points of the flow. Upon differentiating ψ with respect to x we find that the vertical velocity is zero when $z = -1$, $x = 0$ or when the condition

$$x^2 + z^2 = 4 \tag{22}$$

is satisfied. Differentiating ψ with respect to z and substituting for x we can determine the position of the stagnation points exactly and find that

$$\nabla\psi = \mathbf{0} \quad \text{if} \quad (x, z) = \left(\pm\frac{\sqrt{3-8\gamma}}{1-2\gamma}, \frac{4\gamma-1}{1-2\gamma}\right), \quad 0 \le \gamma < \frac{3}{8}, \tag{23}$$

$$\text{or} \quad (x, z) = (0, z'), \tag{24}$$

where z' is solution to

$$\frac{4(1+z')}{z'(2+z')^2} = \gamma. \tag{25}$$

For $0 < \gamma < 3/8$ the first two constitute saddle points fore and aft the roller, while the third corresponds to a centre vertically above the singularity. When $\gamma = 0$, the centre disappears and the saddle points collapse onto the wall. When γ passes through $3/8$ then these coalesce in a pitchfork bifurcation and only one saddle remains. Since we observe $\gamma \approx 0.1$ in our numerical simulations, we discard this case and obtain a flow field with four topologically distinct regions as discussed in the main text.

The value of the streamfunction at the stagnation points is

$$\psi_0 = \gamma + \frac{1}{2}\log(1-2\gamma) = -\gamma^2 - \frac{4}{3}\gamma^3 + \mathcal{O}(\gamma^4), \tag{26}$$

so that the streamline passing through the stagnation point satisfies $\psi = \psi_0$. We compare the height of this streamline centrally below the singularity (z_0), at the stagnation point (z_*) and far away (z_∞) to understand whether squeezing occurs. As $x \to \infty$ we have

$$\psi = -\gamma(z+1) + 2\frac{(z+1)^2}{x^2} + \mathcal{O}(x^{-4}), \quad \Rightarrow \quad z_\infty = -1 - \frac{1}{2\gamma}\log\left(1-2\gamma\right). \tag{27}$$

At leading order in γ we therefore have $z_\infty = \gamma$. Meanwhile, z_0 satisfies

$$\gamma + \frac{1}{2}\log(1-2\gamma) = \log\frac{1-z_0}{1+z_0} + \frac{2z_0}{1+z_0} - \gamma z_0. \tag{28}$$

Due to the presence of the logarithm, this equation does not have an analytic solution. However, we may expand for small z_0 and γ and find

$$-\gamma^2 - \frac{4}{3}\gamma^3 + \cdots = -\gamma z_0 - 2z_0^2 + \frac{4}{3}z_0^3 + \ldots \tag{29}$$

Thus $z_0 \sim \gamma$ at leading order and we can solve a quadratic to find $z_0 = \gamma/2 + O(\gamma^2)$. In summary we have to leading order that

$$z_0 = \frac{1}{2}\gamma, \quad z_* = 2\gamma, \quad z_\infty = \gamma, \quad \psi_0 = -\gamma^2. \tag{30}$$

Thus the streamline coming in from infinity first goes up to twice its original height at the stagnation point before being squeezed down to half its original height below the singularity. As discussed in the main text, this squeezing of streamlines gives rise to irreversible trapping of cargo particles. An illustration is given in Figure S4.

C. With force, $\eta > 0$

In the case that the force is non-zero we have a more complicated streamfunction. In this case the condition for no vertical flow ($\psi_x = 0$) becomes

$$x^2 + \left(z + \frac{2\eta}{1+2\eta}\right)^2 = 4\left(\frac{1+\eta}{1+2\eta}\right)^2. \tag{31}$$

Using this we find that the condition for no lateral velocity ($\psi_z = 0$) becomes

$$-\gamma + \frac{(1+2\eta)(z+1)}{2(z+2)} + \frac{\eta}{2}\log\left(\frac{(1+\eta)(z+2)}{1-\eta z}\right) = 0. \tag{32}$$

This is now a transcendental equation for z with no analytical solution. To make progress, we expand this for small γ and find that

$$z_* = \frac{2(1+\eta)}{(1+2\eta)^2}\gamma + \mathcal{O}(\gamma^2), \quad \psi_0 = -\frac{1+\eta}{(1+2\eta)^2}\gamma^2 + \mathcal{O}(\gamma^3). \tag{33}$$

For as $x \to \infty$ we have

$$\psi = -\gamma(z+1) + \frac{(2+4\eta)(z+1)^2}{x^2} + \mathcal{O}(x^{-4}), \tag{34}$$

so that $z_\infty = (1+\eta)\gamma/(1+2\eta)^2 + \mathcal{O}(\gamma^2)$. For z_0 we find

$$-\frac{1+\eta}{(1+2\eta)^2}\gamma^2 + \mathcal{O}(\gamma^3) = -\gamma z_0 - 2z_0^2 + \frac{4(1+\eta)}{3}z_0^3 + \mathcal{O}(z_0^4) \tag{35}$$

so that to leading order $z_0 = \gamma/2(1+2\eta)$. In summary,

$$z_0 = \frac{1}{2+4\eta}\gamma, \quad z_* = \frac{2(1+\eta)}{(1+2\eta)^2}\gamma, \quad z_\infty = \frac{1+\eta}{(1+2\eta)^2}\gamma, \quad \psi_0 = -\frac{1+\eta}{(1+2\eta)^2}\gamma^2, \tag{36}$$

as quoted in the main text. As expected, we recover our previous results if we set $\eta = 0$. We also have

$$\frac{z_0}{z_\infty} = \frac{1+2\eta}{2+2\eta} \leq 1 \tag{37}$$

for $\eta \geq 0$, therefore squeezing always occurs in the presence of a force. However, the relative extent to which streamlines are squeezed is maximised for a force-free roller. Notably, in the limit $\eta \to \infty$ with γ/η finite, corresponding to a purely translating roller with no rotation we have

$$z_0 = \frac{1}{4\eta}\gamma, \quad z_* = \frac{1}{2\eta}\gamma, \quad z_\infty = \frac{1}{4\eta}\gamma, \quad \psi_0 = -\frac{1}{4\eta}\gamma^2, \tag{38}$$

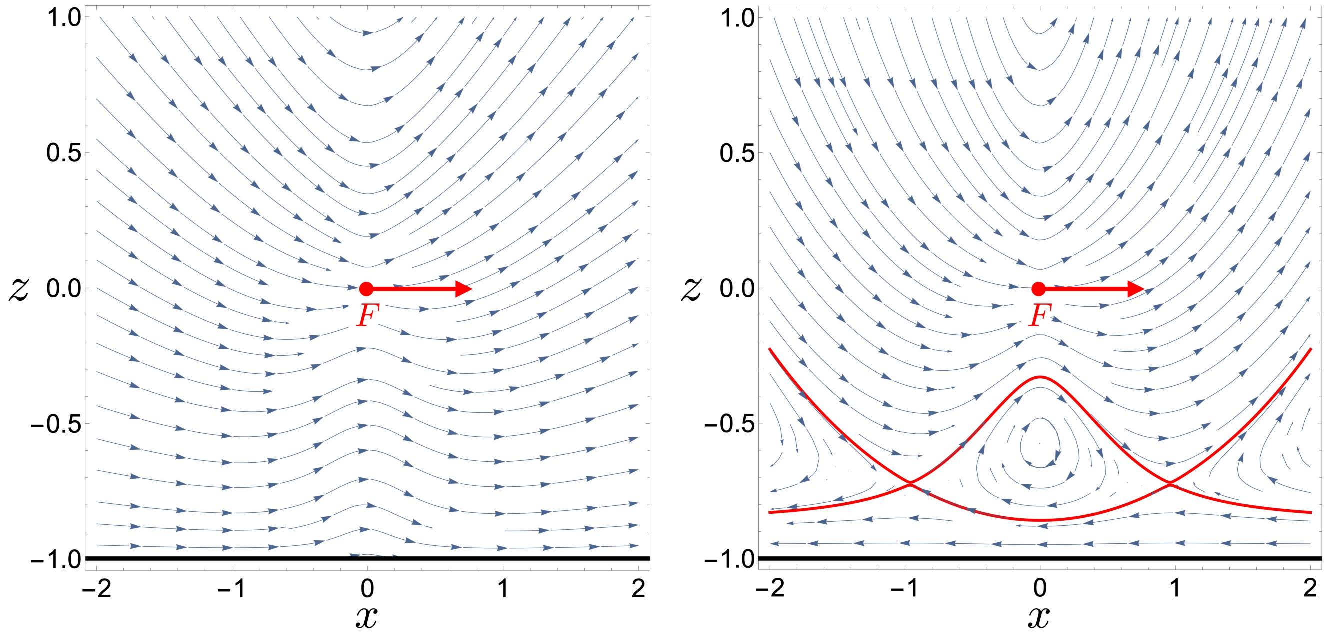

(a) $\gamma/\eta = 0$ (b) $\gamma/\eta = 0.5$

FIG. S5: Streamlines for a force with no rotation (ψ/η for $\eta \to \infty$ and γ/η finite). The separatrix streamline is indicated in bold red. No squeezing occurs, yet a region of closed streamlines exists below the singularity.

indicating that no squeezing occurs. This shows that according to our model rotation is an essential ingredient for entrapment. An illustration is given in Figure S5.

[1] J. Blake and A. Chwang. Fundamental singularities of viscous flow. *Journal of Engineering Mathematics*, 8:23–29, 1974.
[2] A. J. Goldman, R. G. Cox, and H. Brenner. Slow viscous motion of a sphere parallel to a plane wall .2. couette flow. *Chem. Eng. Sci.*, 22(4):653, 1967.
[3] D. Jeffrey and Y. Onishi. The slow motion of a cylinder next to a plane wall. *Quart. J. Mech. Appl. Math.*, 34(2):129, 1981.
[4] C. Pozrikidis. *Boundary integral and singularity methods for linearized viscous flow.* Cambridge University Press, 1992.
[5] J. Tanzosh and H. Stone. A general approach for analyzing the arbitrary motion of a circular disk in a stokes flow. *Chemical engineering communications*, 148:333–346, 1996.